Solute mixing during imbibition and drainage in a macroscopically heterogeneous medium

M. Rossi,[1] P. Lehmann,[1] N. Ursino,[2] O. Ippisch,[3] and H. Flühler[1]

Received 15 February 2005; revised 3 November 2006; accepted 20 November 2006; published 25 April 2007.

[1] We studied the flow of water and the transport of solutes in a heterogeneously packed sand tank by performing transport experiments with a fluorescent tracer. The packing consisted of an inclined, layered sand bedding characterized by a large number of thin layers of three quartz sands of different grain sizes. The purpose was to evaluate to which extent the preceding wetting-draining history affects the mixing of solutes in presence of textural heterogeneities. We irrigated the surface at stepwise increased flow rates (imbibition) and afterward at stepwise decreased flow rates (drainage). At each step the flow rate was kept constant to monitor the transport and spreading of several tracer plumes in the stationary flow field. The results show that during imbibition, mixing at the textural boundaries is hindered and the solutes are funneled through connected preferential flow paths. During drainage we observed enhanced mixing resulting in a definitely less heterogeneous transport regime. These results stress the role of the preceding wetting-draining history for determining the characteristics of solute transport in heterogeneous media. We demonstrate this using the integral mixing characteristics ''dilution index'' and ''reactor ratio,'' which quantify the degree of preferentiality of flow and transport.

Citation: Rossi, M., P. Lehmann, N. Ursino, O. Ippisch, and H. Flühler (2007), Solute mixing during imbibition and drainage in a macroscopically heterogeneous medium, *Water Resour. Res.*, *43*, W04428, doi:10.1029/2005WR004038.

1. Introduction

[2] Natural soils are heterogeneous due to the parent rock material properties and to soil formation processes. Pedogenesis produces layers, lenses and inclusions of different materials whose sizes vary over a wide range. The locally varying hydraulic properties cause, especially under water-unsaturated conditions, a strong variation of the local water velocities. Regions where the water velocity is particularly high compared to spatially averaged flux are often referred to as preferential flow paths. Solute transport in preferential flow paths is characterized by a reduced dilution of the locally high solute concentrations, leading to fast traveling concentration peaks. Therefore, for a realistic description of contaminant transport in the field, it is indispensable to predict the preferentiality of flow and transport. This is even more important when the solid surface in the preferential flow paths and in the by-passed soil matrix differ in terms of contaminant sorption.

[3] Numerous tracer experiments have been carried out at the field scale demonstrating the complexity of flow and transport in heterogeneous soils and the ubiquitous occurrence of preferential flow. For a review on preferential flow we refer to the work of *Jarvis* [2002]. Effects of heterogeneities on unsaturated flow have been studied also by means of numerical experiments [*Russo et al.*, 1989; *Roth*, 1995; *Birkholzer and Tsang*, 1997] and in laboratory experiments using sand tanks of variable sizes [*Wildenschild and Jensen*, 1999; *Ursino et al.*, 2001a]. In sand tank experiments the spatial distribution of the different sands is usually well defined and the boundary conditions well controlled. The data sets produced under laboratory conditions do however not mimic field conditions, but they allow to test model assumptions.

[4] Flow heterogeneity depends on the spatial distribution of water saturation which in turn depends on the imposed flow rate [*Roth*, 1995; *Roth and Hammel*, 1996]. Decreasing the flow rate might do both, enhancing or also diminishing the heterogeneity of the flow field. *Ursino et al.* [2001a] showed that in the heterogeneous structure as used in our experiment the flow field is much more erratic under a low-flow regime.

[5] In the field the input flux always varies with time and causes a continuous sequence of drainage and imbibition regimes. In general, wetting and draining soils cause air entrapment at different scales and prevents on the timescale of the process the equilibration of the air and water phase. The resulting relation between mean water content and matric potential can be described by means of a nonunique water retention curve [*Haines*, 1930; *Hillel*, 1980]. The effect of consecutive drainage and wetting phases on the water retention curve was investigated in laboratory experiments and numerical simulations [*Stauffer and Dracos*, 1986; *Lehmann et al.*, 1998]. In some cases wetting and drainage cause a macroscopically nonunique behavior, such as fingering in sandy soils under dry condition [*Lu et al.*, 1994] or the reduced diversion capacity of capillary barriers

[1]Institute of Terrestrial Ecosystems, Eidgenössische Technische Hochschule Zürich, Zurich, Switzerland.
[2]Dipartimento di Ingegneria Idraulica, Marittima, Ambientale e Geotecnica, Università di Padova, Padua, Italy.
[3]Interdisciplinary Center for Scientific Computing, Ruprecht-Karls-University of Heidelberg, Heidelberg, Germany.

0043-1397/07/2005WR004038$09.00

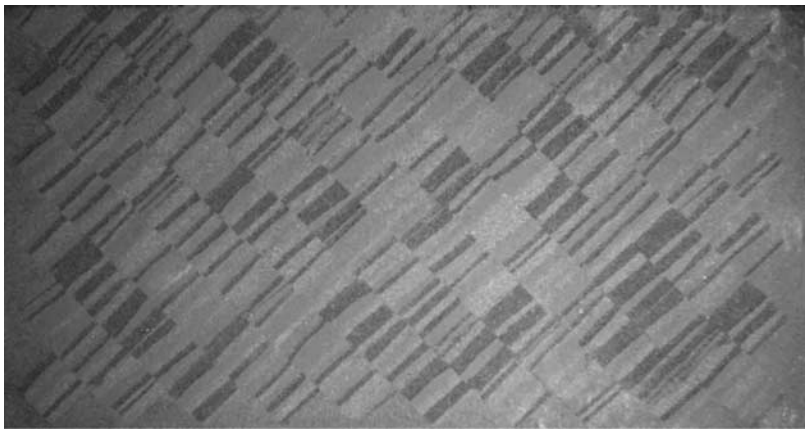

Figure 1. Heterogeneous sand structure used in the experiment. Note the inclined layering and the random location of the individual layers. The length of the layers is constant (5 cm).

under repeated wetting cycles [*Walter et al.*, 2000]. Also homogeneous soils can show a state-dependent anisotropy of the hydraulic conductivity as a result of the spatial variations of the water content [*McCord et al.*, 1991]. *Russo et al.* [1989] carried out a numerical study, analyzing the one-dimensional vertical transport of a nonreactive solute in a heterogeneous profile. In general, the presence of coarse horizontal layers embedded in fine material enhance the lateral dispersion of a vertically advancing plume. We studied the effect of imbibition and drainage on solute transport in an artificial packing of many inclined sand layers. In this case we use the term hysteresis both in a macroscopic sense, for the nonequilibrium of the water distribution between the individual homogeneous layers, and also in a local sense, for the pore-scale hysteresis within these layers. The location, shape and connectivity of the heterogeneities together with the their local hysteresis lead to differently distributed water saturations depending on the preceding wetting-drainage history.

[6] The boundaries between two adjacent materials, hereafter referred to as textural boundaries, play an important role in shaping the flow field. In fact, the accessibility for water (imbibition) or air (drainage) to a region of each homogeneous layer is strongly influenced by the material composition of the neighboring layers. For example, when a fine textured region is in contact with a coarser textured region, water is held in the former by capillary forces [*Miyazaki*, 1988; *Kung*, 1990; *Schroth et al.*, 1998]. Water enters the coarser material at pressure heads less negative than the water entry value [*Hillel and Baker*, 1988]. Therefore textural boundaries may confine water in channels and contribute to the formation of preferential flow paths. Air might get entrapped in pockets of coarse material in the course of imbibition if they are encased by finer material.

[7] At such textural interfaces tracer plumes are getting only slightly diluted. The mean concentration remains high in the fast flow paths and the solutes spread much more unevenly in space. *Kitanidis* [1994] analyzed the difference between spreading of a plume of solute, described by the second spatial moments, and its dilution. He stressed the fact that a plume can be widely spread, i.e., tracer can be found far from its center of mass, but at the same time not becoming diluted. In other contexts, such a mixing regime is being referred to as preferential transport. Kitanidis quantified the degree of dilution by defining the dilution index, which can be interpreted as mixing entropy [*Jaynes*, 1957]. He also introduced the reactor ratio, that measures the entropy of the plume relative to its possible maximum entropy for a given experimental constellation. The concept of entropy can be used to quantify the complexity of the geometry of the transport field [*Faybishenko et al.*, 2000; *Mays et al.*, 2002]. *Ursino et al.* [2001b] found that the entropy of solute plumes may assume comparable values under different flow rates and thus under different transport regimes, whereas the maximum entropy and thus the reactor ratio may considerably differ depending on the controlling transport process. A low reactor ratio indicates that solute mixing at the microscopic scale is impeded. A high reactor ratio refers to a situation of unhindered mixing. A reactor ratio of 1 defines the ideal Gaussian mixing.

[8] Using the artificial sand bedding already used by *Ursino et al.* [2001a], we focus on the role of heterogeneity on the solute mixing during imbibition and drainage. We characterized the transport properties of the medium for consecutive stationary flow fields by tracing water with a fairly mobile fluorescent solute. We quantified the reactor ratio of solute plumes and tested whether it depends on the preceding wetting-draining history.

2. Materials and Methods

2.1. Tank Experiment

[9] The experiment was conducted using the sand structure assembled by *Ursino et al.* [2001a, 2001b]. The sand structure was composed of layered cubes of $5 \times 5 \times 5$ cm, obtained using fine, medium, and coarse quartz sand with particle sizes of 0.08–0.2 mm, 0.1–0.5 mm, and 0.3–0.9 mm, respectively. The layers were 0.5 cm thick and their sequence in the cubes was random. To assign a type of sand to each location a random sequence of the numbers 1, 2, and 3 was produced, with these numbers representing one type of sand. The cubes were assembled in a tank ($75 \times 40 \times 5$ cm) at an inclination of 45°. The front and the back walls of the tank consisted of glass plates of 12 mm thickness. The space between the cube structure and the sidewalls was filled with a mixture of the three sands in equal proportions. Figure 1 shows a picture of the sand structure visible through the glass wall. A layer of fine gravel (3–5 mm

Table 1. Hydraulic Properties of the Three Quartz Sands, the Mixed Sand, Filters, and Fine Gravel[a]

Sand Type	$K_{s,w}$, m/s	$K_{s,d}$, m/s	θ_s	α_w, m^{-1}	α_d, m^{-1}	n	τ[b]	θ_r
Coarse	$5.2\ 10^{-4}$	$5.6\ 10^{-4}$	0.32	11.0	6.3	6.3[c]	0.5	0.02
Intermediate	$1.3\ 10^{-4}$	$1.5\ 10^{-4}$	0.33	7.6	3.6	9.2	0.5	0.02
Fine	$3.5\ 10^{-5}$	$4.4\ 10^{-5}$	0.35	4.7	2.0	6.6	0.5	0.00
Mixed sand	$1.3\ 10^{-4}$	$1.5\ 10^{-4}$	0.33	7.6	3.6	3.0	0.5	0.02
Filters	$4.8\ 10^{-6}$	$4.8\ 10^{-8}$	0.40	0.5	0.5	8.0	0.5	0.00
Fine gravel	$5.2\ 10^{-3}$	$5.2\ 10^{-3}$	0.40	10.0	10.0	6.0	0.5	0.00

[a]Subscripts *w* and *d* refer to wetting and drainage, respectively.
[b]Assumed values.
[c]Parameter determined by the group of Soil Science and Soil Physics, TU Braunschweig, Germany.

particle size) covered the upper side of the tank structure in order to redistribute water.

[10] The hydraulic properties of the three quartz sands were determined by *Ursino and Gimmi* [2004] by multistep inflow and outflow experiments in columns. The parameters of the water retention function [*van Genuchten*, 1980] and the hydraulic conductivity were obtained by inverse modeling. They accounted also for the local hysteresis of the sands producing two α parameters and two saturated hydraulic conductivities per material, namely α_w and α_d, and $K_{s,w}$ and $K_{s,d}$ for wetting and drainage, respectively. The determination of n for the coarse sand was problematic [*Ursino and Gimmi*, 2004]. For this reason we rely on the value of n determined by the group of Soil Science and Soil Physics at the Technical University of Braunschweig, Germany (A. Peters and W. Durner, oral communication, 2006). The hydraulic properties for the three sands are listed in Table 1. In Table 1 we list also the hydraulic properties of the mixed sand used at the tank boundaries, those of the fine gravel and of the filters (bronze porous plates). For mixed sand and fine gravel these values were not measured but estimated on the basis of the parameters of the other sands. The n parameter of the mixed sand, that expresses the broadness of the pore size distribution, was set to 3, a value lower than the n values of all the other sands because being a mixture we expect a broader pore size distribution as a consequence of a broader particle size distribution. The intermediate sand has broad particle size distribution, that overlaps with the range of variation of the particle sizes of the fine and coarse sand. We set α for the mixed sand equal to that of the intermediate sand. The chance that the addition of the coarser fraction would lead a higher α is low, because this would only occur in case of a connected path of poorly mixed coarse sand. Since the saturated conductivity K_s is closely related to α [*Carsel and Parrish*, 1988], we set the saturated conductivity of the mixed sand equal to that of the intermediate sand. The saturated conductivity of the filters was measured before the experiment started ($K_s = 4.8\ 10^{-6}$ m/s).

[11] Transport experiments were performed applying a fluorescent tracer onto the upper surface of the sand structure using a cylindrical stick of a frozen tracer solution at a concentration of 0.5 g/L of Acid Yellow (Aakash Chemicals and Dye-Stuffs, Inc., Glendale Heights, Illinois). The stick was 5 cm long and with a diameter of 0.4 cm. When put onto the surface, its circular bases were in contact with the glass walls of the tank, generating a point source at the 40 × 75 cm glass wall. The sticks melted and the solution seeped into the sand within less than one minute after application, a time much shorter than the plume traveltime. Therefore we consider it as an instantaneous tracer pulse injection and assume that the melting rate had negligible effects on the plume behavior. The distribution of the fluorescent tracer was imaged through the glass wall. It was excited by illuminating the wall with light of 420 nm wavelength, obtained by optical filtering of the light emitted by a Xenon lamp. The tank was imaged with a CCD camera through a filter selecting the wavelength of 520 nm, the emission wavelength of the tracer. The experimental setup used for imaging the tank is described in the work of *Aeby et al.* [2001].

[12] The sand packing was homogeneous in the direction of side wall to sidewall. Therefore the imaged side of the tank (Figure 1) can be considered as a two-dimensional transport domain in which we observed the spreading of tracer pulses.

[13] A steady flux was applied onto the upper surface of the tank with a moving dripping bar mounted above the tank. The 5 cm long dripper consisted of seven syringe needles. The dripping rate and the bar velocity were adjustable. At the bottom of the tank we used bronze porous plates to maintain a pressure head that ranged from −5 to −40 cm, depending on the flow rate to be applied.

[14] In order to perform transport experiments during imbibition, the tank has been initially dried with hot air injected through the porous plates. The experiment was started with water applied onto the dry sand at a low-flow rate. The sequence of the applied flow rates is given in Table 2. The flow rate was kept constant for the duration of each experimental step. The tracer pulses were applied at different locations after establishing stationary flow, at most three pulses at once to avoid overlapping while being leached through the sand bedding. After completion of the imbibition experiments at low- and intermediate-flow rates, saturation was achieved by first draining the tank and drying it, by flushing it with hot air from the bottom, then with CO_2, and finally saturating it slowly with water from the bottom. Trapped CO_2 bubbles dissolve in water and the CO_2 enriched water was leached out in the course of establishing steady state flow. The pressure of the CO_2 was controlled using a water column in parallel with a CO_2 bottle. We kept the flushing pressure at the porous plates at approximately 10 hPa in order to avoid disturbances of the packing. The CO_2 pressure drop across the porous plates reduced the CO_2 pressure gradient through the sand packing to definitely less the 10 hPa.

[15] After the saturation procedure a transport experiment was performed at the constant flow rate of 4.3×10^{-6} m/s

Table 2. Applied Flow Rates and the Number of the Applied Tracer Plumes

Experiment	Flow Rate j_w, 10^{-6} m/s	Pressure Head h at the Lower Boundary, m	Number of Applied Plumes
Imbibition low-flow rate (ILFR)	1.2	−0.05	5
Imbibition intermediate-flow rate (IIFR)	3.2	−0.05	10
Saturation 1 (S1)	4.3	−0.40	3
Saturation 2 (S2)	9.3	−0.12	3
Drainage intermediate-flow rate (DIFR)	2.5	−0.27	3
Drainage low-flow rate (DLFR)	1.0	−0.40	6

(Table 2). Because of a technical problem with the CCD camera the experiment was interrupted. It was resumed for the second transport experiment under saturated conditions that was again reached by the same saturation procedure as described above. At this state a flow rate of 9.3×10^{-6} m/s could be maintained. The difference in the achieved flow rates is probably caused by a difference in water content. Hence the system was probably close to but not at full saturation. Close to saturation minor changes of water content result in large variation of conductivities.

[16] During the drainage experiment the conductivity of the bronze filters decreased in time, due to partial clogging. To keep the water content constant we adjusted the inflow according to the outflow and by increasing the applied suction at the bottom of the tank. The entire experiment including the preparatory phase of establishing the steady flow and repair of the CCD camera lasted 11 months.

[17] At each flow rate we monitored from 5 to 10 tracer plumes (Table 2). A single plume is one realization of the transport process. The plumes observed at the same flow conditions are a small statistical ensemble whose mean properties can be used to characterize the transport regime.

2.2. Image Analysis

[18] The images of the tank obtained with the CCD camera are grey scale pictures of 1136×620 pixels with a 16 bit digitization. The imaged area was 75 cm wide and 40 cm high, thus the images have a resolution of about 0.004 cm^2/pixel.

[19] At low dye concentrations the relationship between solute concentration and intensity of the emitted light is linear [*Aeby et al.*, 2001]. At higher concentrations this relationship is nonlinear, with a decreasing slope toward higher concentrations. Using a linear dependence for high concentrations values leads to an underestimation of the concentration difference for a given difference in emitted light. In the transport experiments we performed at low saturation, the flow paths were narrow and the plumes did not sufficiently dilute. Therefore we use a power law to relate the dye concentration and intensity of the emitted light:

$$I_{em}(x,z) \propto I_{exc}(x,z)c(x,z)^{\gamma}, \tag{1}$$

with $\gamma \in (0,1)$, as the nonlinear calibration parameter. In equation (1) I_{em} is the intensity of emitted light recorded by the CCD camera, $I_{exc}(x,z)$ is the intensity of exciting light and $c(x,z)$ is the concentration of the fluorescent tracer.

[20] To extract a concentration map from the images, we eliminated the dependence on the exciting light from equation (1) by applying the correction procedure described in the work of *Aeby et al.* [2001]. This procedure accounts for the spatially nonuniform illumination and for the spatially varying roughness and optical properties of the imaged surface. Studies were performed in order to assess the effect of water content and soil type on dye tracer fluorescence [*Bänninger et al.*, 2005] and to evaluate the uncertainties on dye concentration estimations [*Vanderborght et al.*, 2002].

[21] After correction, the grey value f of the image at location (x, z) is proportional only to c^{γ} at that particular location:

$$f(x,z) \propto c(x,z)^{\gamma}. \tag{2}$$

From $f(x,z)$ we obtain the total mass M of the plume (zeroth spatial moment) and by normalizing the concentration, the probability distribution of the dye particle position $p(x,z)$:

$$M = \int\int_{\Omega} f^{\frac{1}{\gamma}}(x,z)dxdz, \tag{3}$$

$$p(x,z) = \frac{f^{\frac{1}{\gamma}}(x,z)}{\int\int_{\Omega} f^{\frac{1}{\gamma}}(x,z)dxdz}, \tag{4}$$

The coordinates X and Z of the plume's center of mass are

$$X = \int\int_{\Omega} x\,p(x,z)\,dxdz, \tag{5}$$

$$Z = \int\int_{\Omega} z\,p(x,z)\,dxdz. \tag{6}$$

We then calculate the components of the spreading tensor of the plume:

$$XX = \int\int_{\Omega} (x-X)^2\,p(x,z)\,dxdz, \tag{7}$$

$$ZZ = \int\int_{\Omega} (z-Z)^2\,p(x,z)\,dxdz, \tag{8}$$

$$XZ = \int\int_{\Omega} (x-X)(z-Z)\,p(x,z)\,dxdz. \tag{9}$$

The integrals were computed over the region Ω covered by the plume. Note that the proportionality constant in equation (2) is canceled in equation (4) and all the moments can be calculated without determining its value.

[22] The parameter γ equation (2) is determined for each individual plume using a fitting procedure under the constraint that the plume mass must remain constant in time. The resulting γ values differ somewhat but plumes belonging to the same flow rate show similar γ values. The detectability of the dilute concentrations at the periphery of a plume varies with the sand type and the saturation degree. Hence the possible variation of the detection limit combined with the assumption that the mass M must be constant might explain the variation of γ through the different flow rates.

[23] The effect of the uncertainty in the determination of γ was evaluated (see section 3.3.1) by comparing the dilution of the plumes with the limiting case of $\gamma = 1$, i.e., when the nonlinear dependence of fluorescent emission intensity on concentration is ignored.

[24] The evolving plumes were regularly imaged on their way down through the tank. From this we obtained the velocity of the center of mass and measured the plume dilution as a function of time.

2.3. Reactor Ratio and Dilution Index

[25] The solute distribution of a plume moving through a heterogeneous medium is not Gaussian as expected for a plume moving through a homogeneous medium. For this reason, the first and the second spatial moments, that describe the position of the center of mass of the plume and its spreading, do not provide a sufficient description of the plume geometry. We therefore calculated, in addition to the zeroth, first, and second moments, the dilution index and the related quantity defined as reactor ratio [*Kitanidis*, 1994].

[26] The dilution index was derived based on the concept of entropy of the probability distribution of the solute molecules [*Kitanidis*, 1994; *Beckie*, 1998]. The probability distribution $p(x,z)$ of solute molecule position is obtained from the concentration distribution $c(x,z)$ normalized with the plume mass:

$$p(x,z) = \frac{c(x,z)}{\int\int_{\Omega} c(x,z)dxdz}, \tag{10}$$

where Ω is the plume area. The entropy of the probability distribution is

$$H = -\int\int_{\Omega} p(x,z)\log p(x,z)dxdz. \tag{11}$$

Evolving toward equilibrium the solute molecules tend to spread more homogeneously over the entire transport domain and the entropy of the solute distribution increases.

[27] The dilution index E is defined as [*Kitanidis*, 1994]

$$E = exp(H). \tag{12}$$

The index E increases with increasing dilution and reaches its maximum at equilibrium.

[28] For a solute plume of given centroid position and spreading, the probability distribution which maximizes the dilution index is computed by using the observed center of mass and spreading as constraints. The resulting probability distribution is Gaussian and the value of the corresponding dilution index is

$$E_{\max} = 2\pi \exp\left\{\left(XX \cdot ZZ - (XZ)^2\right)^{1/2}\right\}, \tag{13}$$

where XX, ZZ and XZ are the second spatial moments (equations (7), (8), and (9)). The quantity $E_{\max}$ is the maximum dilution index describing an ideally mixed plume.

[29] The actual mixing of the observed plume is compared to that of a Gaussian plume, having the same centroid position and the same second spatial moments as the observed plume. A Gaussian plume having the same first and second moments represents the highest possible degree of mixing under the given experimental conditions. The deviation of the actual degree of dilution from that expected under ideal mixing conditions can be quantified with the reactor ratio:

$$r = E/E_{\max}. \tag{14}$$

The reactor ratio assumes values from 0 to 1; the value 1 characterizes maximum dilution at that particular traveltime.

[30] For heterogeneous media, as in case of our experiment, the plume is generally far from equilibrium. We therefore expect the reactor ratio of the observed solute plumes to be less than one. In the following we will show how the reactor ratio changes from imbibition to drainage under various flow conditions.

3. Results and Discussion

[31] Under the six flow conditions (Table 2), the solute plumes show very different features. In Figure 2 we show six examples of plumes, one for each flow condition.

[32] At the low-flow rate established under imbibition conditions (Figure 2a) the flow field exhibits distinct preferential flow paths following the fine sand layers. The coarser grained layers are nonconductive. During the following intermediate-flow rate (Figure 2c) preferential flow paths still prevail but they include layers of fine as well as medium sand. The solute passes through the boundaries between these two sands while the boundaries facing coarse sand still act as capillary barriers. In these two flow rates established in the imbibition sequence, the heterogeneity confines water and solutes in channels. The diffusion of the solute at the capillary barrier is too small to allow equilibration of the solute concentration transversely to the flow direction. The sharp borders of plumes along preferential flow paths correspond to nonequilibrated solute concentrations, i.e., an impeded local dilution.

[33] During the two conditions close to saturation (Figures 2e and 2f) all three sands are conductive and preferentiality of flow was not detected. The solute mixing is thorough and the solute concentrations are diluted making the plume boundaries fuzzy. At the intermediate-flow rate following saturation (drainage cycle) (Figure 2d) we still observe a thorough mixing as observed at saturation. At the following low-flow rate (Figure 2b) the preferentiality of flow paths is reestablished but less pronounced as observed at the low-flow rate of the imbibition branch. The bound-

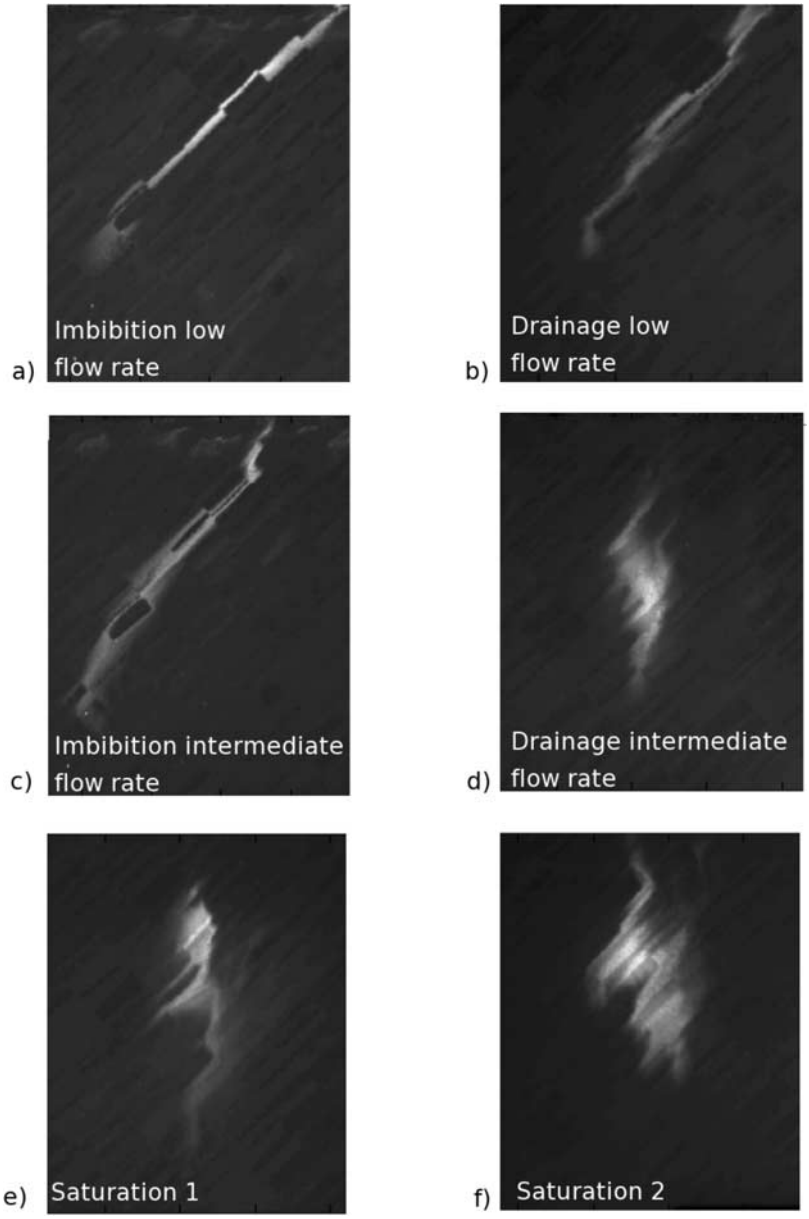

Figure 2. Plumes observed at various flow rates during imbibition, during drainage, and under saturated conditions. In the images the plumes have a higher intensity (emitted fluorescent radiation) compared to the dark background.

aries of the plumes are more fuzzy indicating a better solute mixing.

[34] To support the observation that preferential flow is developing mainly through the finer sand layers at certain flow rates, we quantified the contribution of each of the three sands to solute transport during each experiment. Therefore, for each plume, the binary images of all time steps were added up and the resulting total area was intersected with the map of the fine, medium, and coarse sand (superposition of total area covered by the plume and textural maps). The obtained areal fractions of the three sands for each plume belonging to the same flow rate were added up. The results are shown in Figure 3.

[35] The analysis shows the transition from water-unsaturated to water-saturated conditions. Comparing the results obtained for drainage and for imbibition we note that the major difference is observed at intermediate-flow rates (Figures 3c and 3d). At low-flow rates (Figures 3a and 3b) and also under the two saturation conditions (Figures 3e and 3f), the areal fractions of the various sand types being stained do not differ significantly. Comparing Figures 2a and 2b, a difference is visible in the fuzziness of the plume fringe across the textural boundaries. The fringe area is too small to discriminate the two mixing conditions with this method. As already observed, the flow field at intermediate-flow rate during drainage conditions does not significantly differ from that observed at saturation. In contrast, the intermediate-flow rate during imbibition produced a mixing regime that is more similar to that of the low-flow rate.

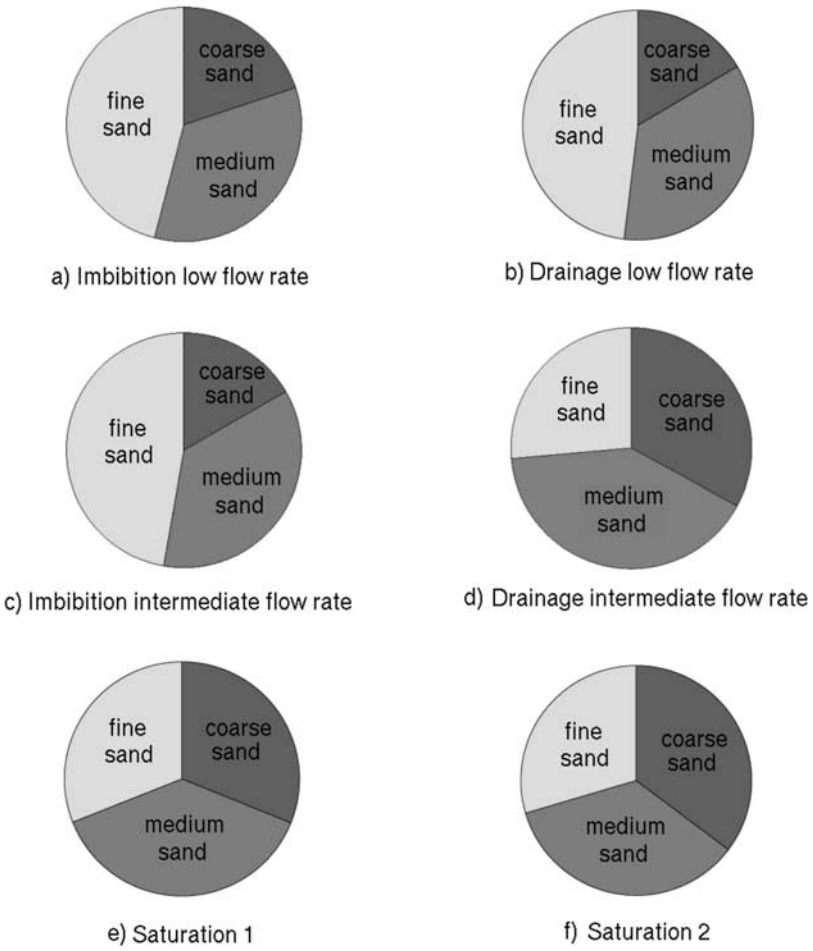

Figure 3. Visibly stained sand fractions contributing to transport during imbibition, during drainage, and under saturated conditions.

3.1. Analysis of Centroid Velocities

[36] From the images we computed the first spatial moments, coordinates of the position of the center of mass, as a function of time of individual plumes. The observation was terminated when the plume reached the region close to the tank bottom when its shape became substantially deformed. The total time of observation varies among the plumes due to the velocities of their center of mass.

[37] Figure 4 shows the vertical displacement of the center of mass with time for the observed plumes, grouped as in Table 2. By linearly fitting these curves we obtained the mean vertical velocity v_z [m/s] of the individual plumes. Each plume is a single realization of the observed transport regime, being applied under the same boundary conditions. In Table 3 the mean velocity and the corresponding variation coefficient for the six ensembles of plumes are shown.

[38] During imbibition the variance of the mean velocities systematically decreases with increasing flow rate from a high value at low-flow rate to a minimum at saturation. In the course of drainage the variance of the mean velocities increases, reaching again a high value at low-flow rate. During drainage at intermediate-flow rate, the coefficient of variation is small compared to the intermediate-flow rate during imbibition and makes this case more similar to the saturation cases confirming the conclusions drawn by observations of the images in Figure 2, despite the small number of plumes and the less reliable statistics. The high variance at low-flow rate, both at drainage and imbibition, is a consequence of the heterogeneity of the flow field. When the plumes are transported along preferential flow paths the velocity primarily depends on the geometry and especially on the connectivity of the flow paths. As the water content of the coarser materials rises the sand bedding behaves as a quasi-homogeneous medium. The tracer is being transported in a wide and fuzzy flow region and not along sharply delimited flow paths, probably reflecting a small variation in water content across the various layers. Because of the increased homogeneity of the medium, the analyzed plumes behave as a statistical ensemble and their mean properties are representative of a given flow and transport regime.

3.2. Estimating the Mean Water Saturation

[39] We estimated the mean water saturation of the tank from numerical simulations. The water flow is simulated using the mixed form of Richards equation:

$$\frac{\partial \theta}{\partial t} = \nabla \cdot [K(\theta)\nabla h] - \frac{\partial K(\theta)}{\partial z}, \qquad (15)$$

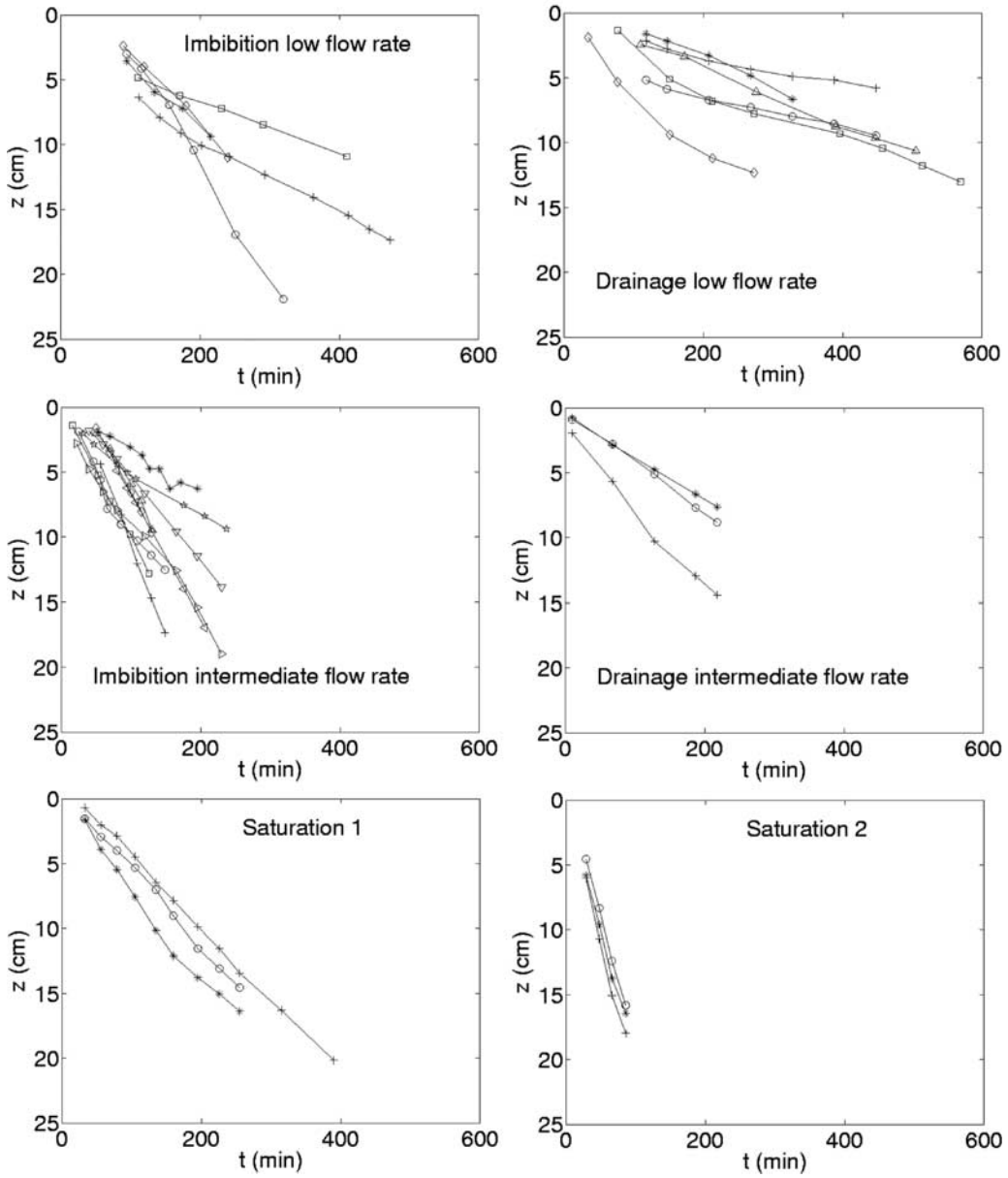

Figure 4. Vertical displacement of the center of mass as a function of time for plumes observed at various flow rates during imbibition, during drainage, and under saturated conditions (different symbols correspond to different plumes).

where h is the matric hydraulic head and z the vertical coordinate directed downward. Richards equation is solved for the primary variable h with a new numerical code, which is optimized for numerical stability even in presence of sharp discontinuities of the hydraulic properties. Hence it is well suited for modeling microscopic redistribution processes in structured porous media. The problems in solving the flow field in the sand tank structure addressed by *Ursino and Gimmi* [2004] have been solved. The model uses a cell-centered finite volume scheme, full upwinding in space, and an implicit Euler scheme in time. The nonlinear equations resulting from discretization of equation (15) are linearized by an incomplete Newton method with line search. The linear equations are solved with an algebraic multigrid solver. For the time solver the time step is automatically adapted.

[40] The model parameters are the saturated conductivity K_s, the van Genuchten parameters, θ_s (water content at saturation), θ_r (residual water content), n (pore space index) and α. The tortuosity τ used in the Mualem model was set to 0.5. In order to solve the flow field we produced a map of the packed sand structure, i.e., a gray scale image where each gray value corresponds to one of the three sand types and, in addition, to the fine gravel layer at the surface and of the mixed sand at the lateral tank boundaries. Given the digital image of the sand structure, the textural map was obtained by using a computer program that allowed to follow the actual contour of each sand layer and to assign to each graphically defined layer the proper gray value. This method reduced the number of not classified or misclassified pixels compared to the sand recognition methods based

Table 3. Ensemble Mean Velocities and Relative Variation of the Velocities

Experiment	j_w, 10^{-6} m/s	$\bar{v}_z$, 10^{-6} m/s	Variation Coefficient of $\bar{v}_z$ ($\sigma_v/\bar{v}_z$)
Imbibition low-flow rate	1.2	8.0	0.55
Imbibition intermediate-flow rate	3.2	13.0	0.40
Saturation 1	4.3	10.0	0.10
Saturation 2	9.3	31.0	0.06
Drainage intermediate-flow rate	2.5	7.3	0.29
Drainage low-flow rate	1.0	3.7	0.53

on image analysis [*Gimmi and Ursino*, 2004]. This procedure was possible because the various sand types were clearly distinguishable by eye. The disadvantage of this method is that it cannot be automated.

[41] The map had a size of 1136 × 620 pixels and a resolution of 0.004 cm^2/pixel. We simulated drainage and imbibition by using two different values for K_s and α as indicated in Table 1. The effect of the clogging of the filters during the drainage phase was accounted for by using in the numerical simulation diminished values of their conductivity. We used the value 9.6×10^{-9} m/s for the simulation of saturation 1 and drainage intermediate- and low-flow rates. For saturation 2 we used a slightly increased value 4.8×10^{-8} m/s, because we hypothesize that the procedure of flushing with CO_2 reduced temporary the clogging. The resulting mean saturation of the tank for the six experiments are listed in Table 4.

[42] As expected, at low-flow rate during imbibition the mean saturation is close to 0.33, the value that would result by considering only the fine sand being close to saturation and the remaining sands dry. The mean saturation increases at intermediate-flow rates when the medium sand is activated. The mean saturation at low-flow rate turns out to be higher during drainage than during imbibition, probably due to the coupled effect of local hysteresis of the hydraulic properties of each sand and of the macroscopic hysteresis of the structured soil. The different plume aspect observed during intermediate-flow rate experiments (Figures 2c and 2d) is caused by high water content and by the presence of more water in the coarser layers compared to imbibition. At low-flow rate the difference in the mean saturation between drainage and imbibition is smaller. Yet, it affected the transport regime as we already observed (Figure 2).

3.3. Reactor Ratio

[43] The reactor ratio of the observed plumes has been measured as a function of time (Figure 5). Two classes can be distinguished based on the values of the reactor ratio: (1) a high variability with several plumes showing values below 0.5 for the imbibition and the low-flow drainage regime and (2) less variability with very few values below 0.5 for saturation and intermediate-flow rate drainage. At imbibition and drainage at low-flow rate, the high variability of r can be explained by the presence of preferential flow paths. The solute transport is restricted to fine material and more affected by local conditions, as for instance the flow paths connectivity. At saturation and drainage at intermediate-flow rate, the plumes are generally closer to a Gaussian dilution, leading to larger reactor ratios. Plumes do not strictly follow the bedding geometry, can mix at the textural boundaries and move into all three sands. For this reason the reactor ratio varies less as compared to the case of preferential transport. Under all conditions, imbibition, drainage and saturation, most plumes do not reach an asymptotic regime, probably because the transport region from the tank surface to its bottom is still relatively small compared with the correlation lengths of the layered structures. This is the basic problem of preferential flow wherever it is observed.

[44] For further analysis the measured values of the reactor ratio for all plumes were grouped per flow rate. The theoretical range of variation of the reactor ratio (0 to 1) has been divided in five classes and the frequencies of occurrence plotted in histograms. The results are shown in Figure 6. Comparing the histograms for similar flow rates during imbibition and drainage (Figures 6a and 6b and 6c and 6d), we observe that small values of the reactor ratios were more frequent during imbibition, indicating that the degree of dilution is lower than during drainage and the plumes deviate more from the complete (Gaussian) dilution. The limited dilution results from a local mixing process that is hindered by the textural boundaries. On the contrary, during drainage mixing is enhanced.

[45] We do not observe any substantial difference between the results corresponding to the two flow rates under saturated conditions (Figures 6e and 6f); the reactor ratio values assumes high values concentrated in a narrow interval. The reactor ratio remains, however, less than 1, confirming that the transport process is preasymptotic. The variable conductivity values in the sand structure prevents a thorough dilution of the plume. Under these conditions textural boundaries have a marginal effect on the reactor ratio.

3.3.1. Evaluation of Uncertainties on Dilution of the Plumes

[46] We obtained concentration maps from the images using $\gamma = 1$ in equation (2), i.e., approximating the relation between intensity of emitted fluorescent light and concentration assuming a linear dependence. By considering $\gamma = 1$,

Table 4. Mean Water Saturation Estimated With Numerical Simulations of the Five Experimental Conditions

Experiment	Value
ILFR	0.34
IIFR	0.42
S1	1.00
S2	1.00
DIFR	1.00
DLFR	0.39

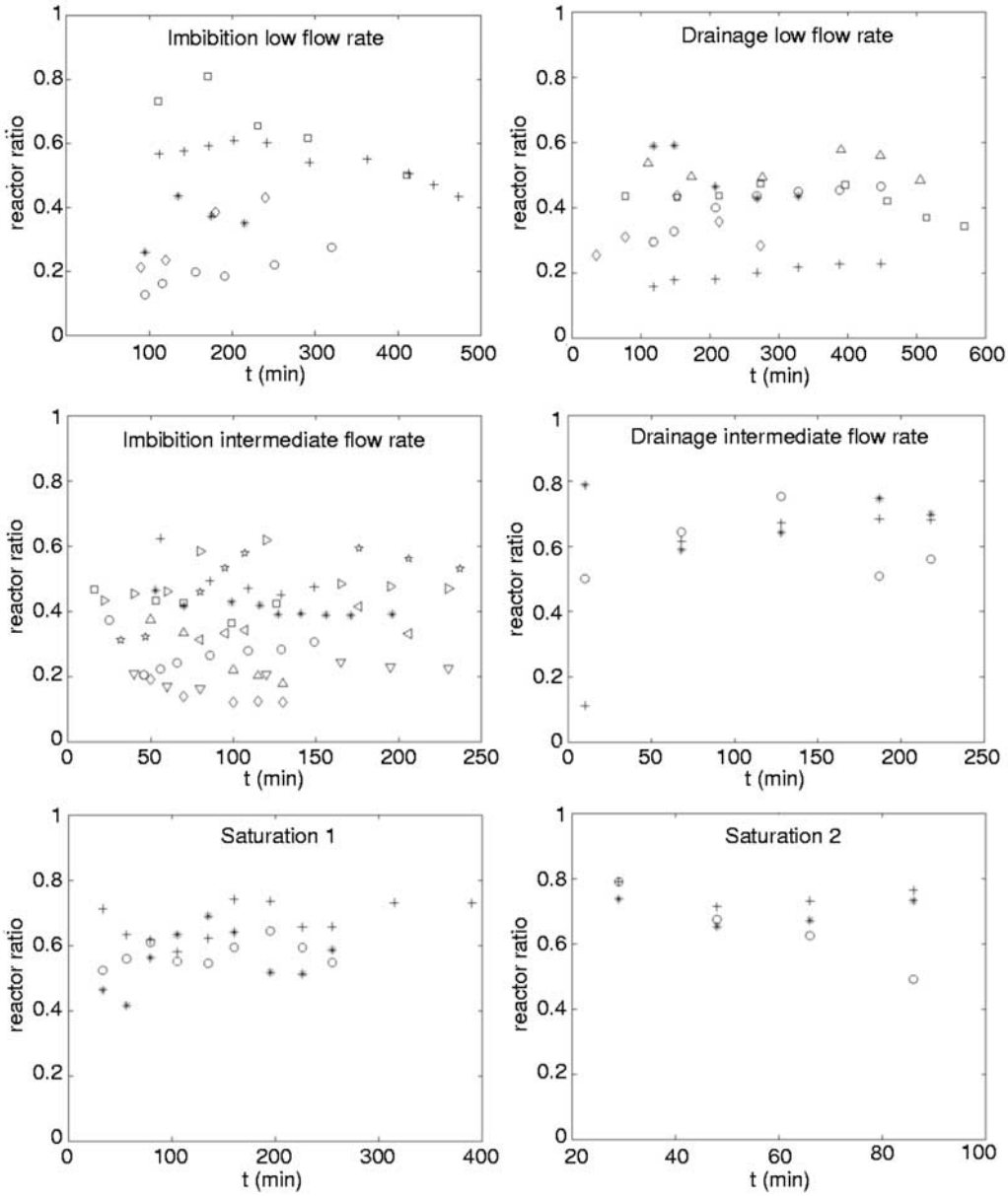

Figure 5. Reactor ratio as a function of time at various flow rates during imbibition, during drainage, and under saturated conditions (different symbols correspond to different plumes).

we analyze the error introduced by assuming a nonlinear calibration function. From these concentration maps we recalculated the reactor ratio of the plumes.

[47] Figure 7 is equivalent to Figure 6 except that the images were interpreted assuming $\gamma = 1$. Figure 7 leads to the same conclusions drawn observing Figure 6. Very similar histograms, being skewed toward low reactor ratio values, characterize the mixing regime at low- and intermediate-flow rates during imbibition. Narrow histograms are found at saturation and histograms skewed toward high reactor ratio values under drainage conditions. The concentration distributions observed at low-flow rates exhibit higher gradients than at high-flow rates, when the distribution are rather smooth. For this reason the choice of of the calibration function affects the histograms more at the low-flow rates.

4. Summary and Conclusions

[48] Nature rarely ever conducts steady flow experiments in the vadose zone. Infiltration and drainage follow each other in very variable sequences. Infiltrating water very heterogeneously displaces the solutes applied or being deposited onto the soil surface. This has been often referred to as preferential flow, but it has been rarely quantified in terms of the degree of preferentiality. Here, we investigate whether the solute mixing regime differs when water moves through a medium whose water distribution is the results of infiltration (imbibition) or redistribution (drainage). We

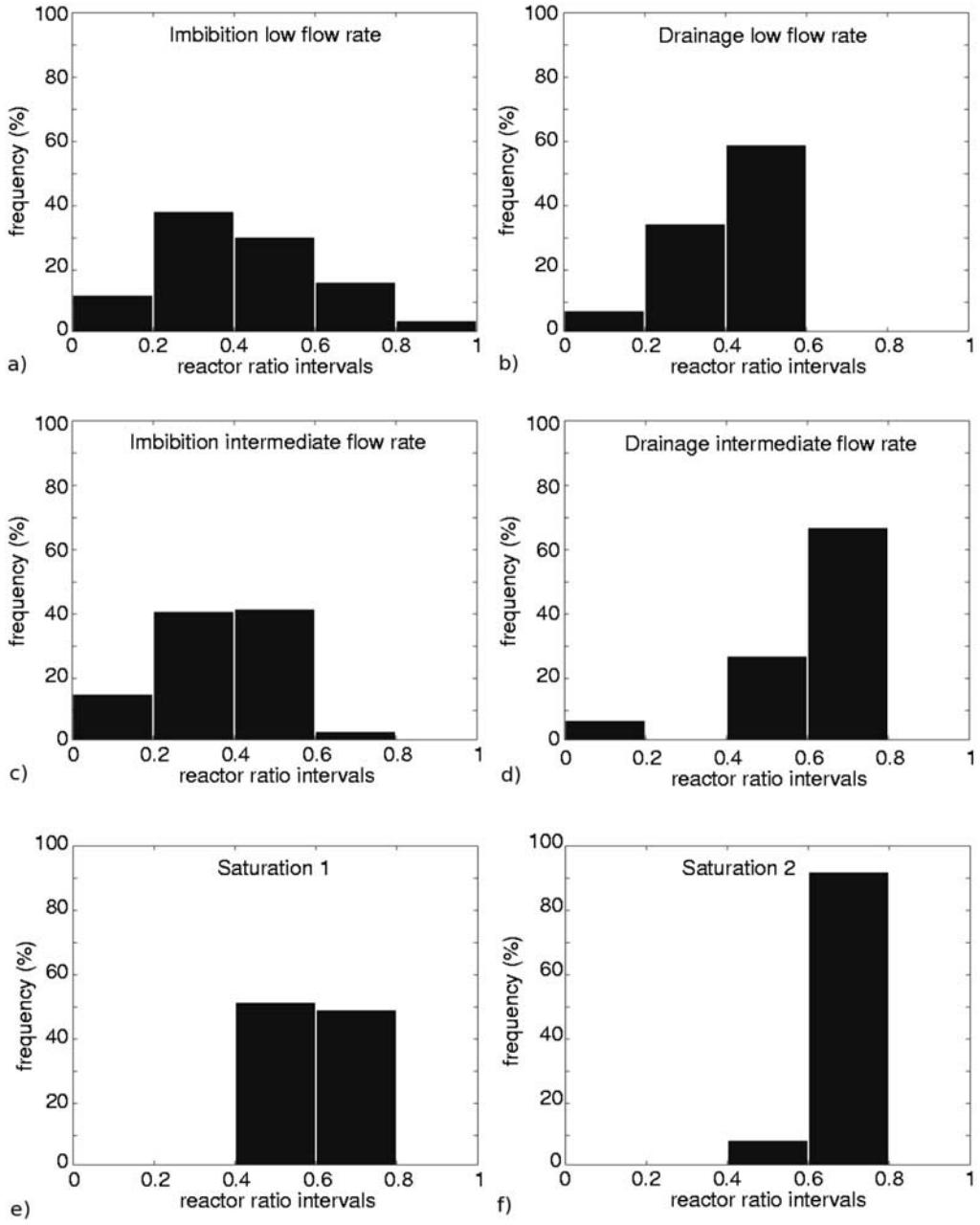

Figure 6. Histograms of the reactor ratio values measured for plumes observed at various flow rates during imbibition, during drainage, and under saturated conditions.

investigated the the difference of the mixing regime under imbibition and drainage conditions in an anisotropic heterogeneous medium using a fairly mobile solute. In particular, we focused on the role of textural boundaries on the mixing of the solute and on the resulting dilution of the solute plumes. The experiment was conducted in the preasymptotic regime of the flow and transport processes, conditions that are often found in the vadose zone in nature.

[49] The degree of preferentiality is expressed in terms of the tracer dilution when the tracer is applied as a point source at the surface of the sand structure. The dilution is determined relative to that occurring under ideal mixing conditions in a homogeneous medium [*Kitanidis*, 1994].

[50] The results tell us the following: (1) Close to saturation and at the intermediate-flow rates established under drainage conditions, we observed a more homogeneous flow field and transport regime, characterized by less variable transport parameters and lower variances of the mean values. (2) In the remaining cases (imbibition low- and intermediate-flow rates and drainage at low-flow rate) the flow field and the transport regime are quite different. The plume velocities and reactor ratios are highly variable, indicating that the flow field needs to be characterized locally. (3) A major hysteretical effect on the mixing regime is visible at the intermediate-flow rates.

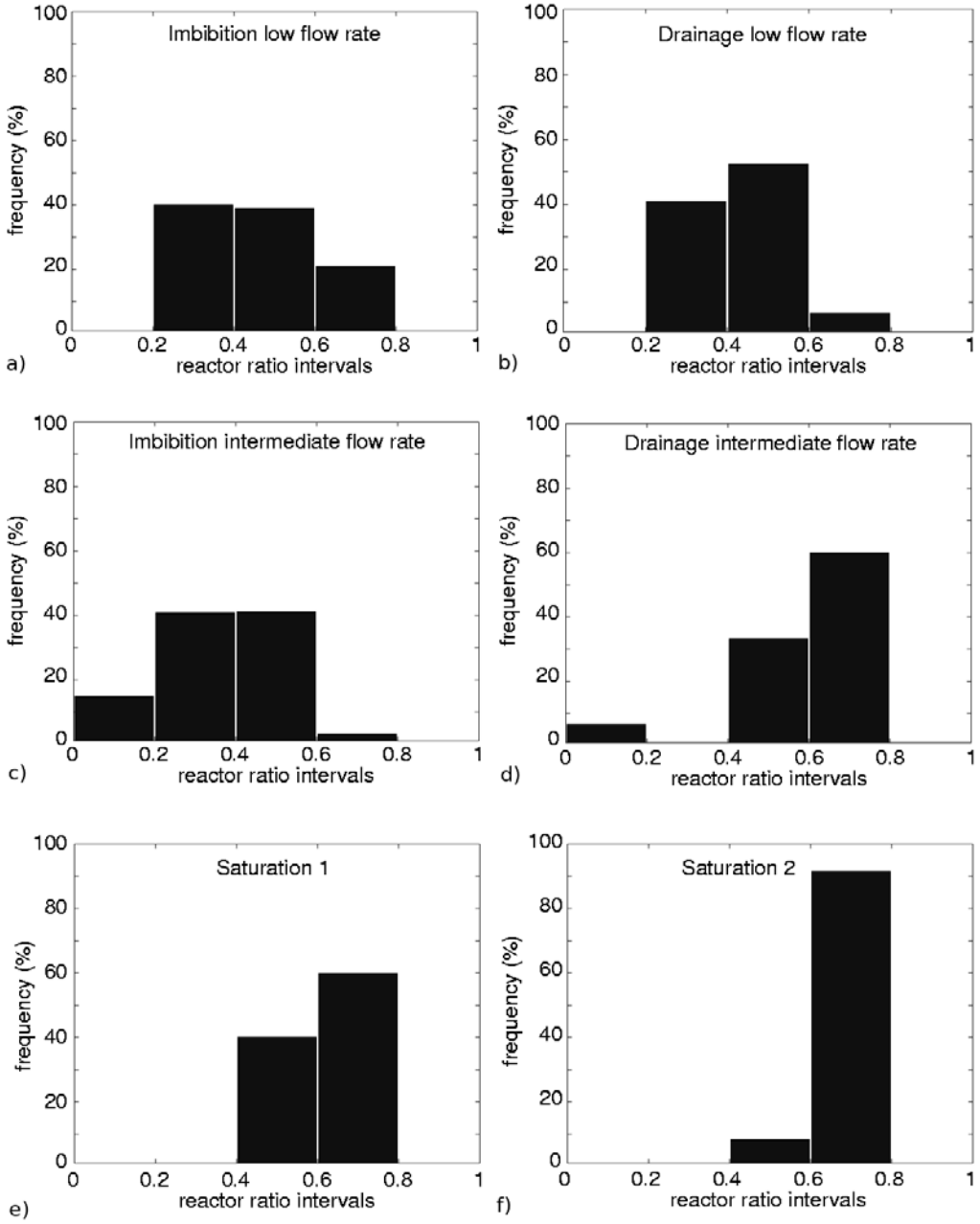

Figure 7. Histograms of the reactor ratio values obtained from images interpreted according to a linear dependence between emitted intensity and concentration.

[51] From a phenomenological point of view we conclude that at comparable flow rates (1) the mixing at the textural boundaries is more impeded during imbibition and the resulting plume dilution is lower than during drainage, (2) under saturated conditions the textural boundaries have a marginal effect on mixing.

[52] We thus conclude that the preceding wetting-draining history might be relevant for predicting the flow field and the solute transport in heterogeneous media. The pore-scale soil water hysteresis of the individual soil materials may play a minor role compared to the global behavior of the macroscopic soil structure, which in our case, was largely determined by the presence of capillary barriers. Including a chemical heterogeneity, closely correlated to the hydraulic heterogeneity, will make these findings even more relevant for practical purposes.

[53] **Acknowledgments.** We thank Hanspeter Läser, who built the tank, for his work and for his enthusiastic and professional support during the long-lasting experiments. Thanks also go to Hannes Wydler for his help in operating the imaging system. The project has been funded by the Swiss National Science Foundation (project 2-77049-01).

References

Aeby, P., U. Zimmerman, D. Braichotte, M. Bundt, F. Moser-Boroumand, H. Wydler, and H. Flühler (2001), Fluorescence imaging of tracer distribution in soils profiles, *Environ. Sci. Technol.*, *35*, 753–760.

Bänninger, D., P. Lehmann, H. Flühler, and M. Guglielmetti (2005), Modelling the effect of soil water content and sorption on dye-tracer fluorescence, *Eur. J. Soil Sci.*, *57*(6), 808–815, doi:10.1111/j.1365-2389.2005.00772.x.

Beckie, R. (1998), Analysis of scale effects in large-scale solute-transport models, in *Scale Dependence and Scale Invariance in Hydrology*, edited by G. Sposito, pp. 314–334, Cambridge Univ. Press, New York.

Birkholzer, J., and C. F. Tsang (1997), Solute channeling in unsaturated heterogeneous porous media, *Water Resour. Res.*, *33*(10), 2221–2238.

Carsel, R., and R. Parrish (1988), Developing joint probability distributions of soil water retention characteristics, *Water Resour. Res.*, *24*, 755–769.

Faybishenko, B., C. Doughty, M. S.J. Long, T. Wood, J. Jacobsen, J. Lore, and P. Zawislanski (2000), Conceptual model of the geometry and physics of water flow in a fractured basalt vadose zone, *Water Resour. Res.*, *36*, 3499–3522.

Gimmi, T., and N. Ursino (2004), Mapping material distribution in a heterogeneous sand tank by image analysis, *Soil Sci. Soc. Am. J.*, *68*, 1508–1514.

Haines, W. (1930), Studies in the physical properties of soil: V. The hysteresis effect in capillary properties and the modes of moisture distribution associated therewith, *J. Agric. Sci.*, *20*, 97–116.

Hillel, D. (1980), *Fundamentals of Soil Physics*, Elsevier, New York.

Hillel, D., and R. Baker (1988), A descriptive theory of fingering during infiltration into layered soils, *Soil Sci.*, *146*, 51–56.

Jarvis, N. (2002), Macropore and preferential flow, in *The Encyclopedia of Agrochemicals*, vol. 3, pp. 1005–1013, edited by J. Plimmer, John Wiley, Hoboken, N. J.

Jaynes, E. T. (1957), Information theory and statistical mechanics, *Phys. Rev.*, *106*, 620–630.

Kitanidis, P. K. (1994), The concept of the dilution index, *Water Resour. Res.*, *30*(7), 2011–2026.

Kung, K. J.-S. (1990), Preferential flow in a sandy vadose zone: 1. Field observation, *Geoderma*, *46*, 51–58.

Lehmann, P., F. Stauffer, C. Hinz, O. Dury, and H. Flühler (1998), Effect of hysteresis on water flow in a sand column with a fluctuating capillary fringe, *J. Contam. Hydrol.*, *33*, 81–100.

Lu, T., W. Biggar, and D. R. Nielsen (1994), Water movement in glass bead porous media: 2. Experiments of infiltration and finger flow, *Water Resour. Res.*, *30*, 3283–3290.

Mays, D., B. A. Faybishenko, and S. Finsterle (2002), Information entropy to measure temporal and spatial complexity of unsaturated flow in heterogeneous media, *Water Resour. Res.*, *38*(12), 1313, doi:10.1029/2001WR001185.

McCord, J. T., D. B. Stephens, and J. L. Wilson (1991), Toward validating: State dependent macroscopic anisotropy in unsaturated media: Field experiments and modeling considerations, *J. Contam. Hydrol.*, *7*, 145–175.

Miyazaki, T. (1988), Water flow in unsaturated soil in layered slopes, *J. Hydrol.*, *102*, 201–214.

Roth, K. (1995), Steady flow in an unsaturated, two-dimensional, macroscopically heterogeneous, Miller-similar medium, *Water Resour. Res.*, *31*, 2127–2140.

Roth, K., and K. Hammel (1996), Transport of conservative chemical through unsaturated two-dimensional Miller-similar medium with steady state flow, *Water Resour. Res.*, *31*, 1653–1663.

Russo, D., W. A. Jury, and G. L. Butters (1989), Numerical analysis of solute transport durin transient irrigation: 1. The effec of hysteresis and profile heterogeneity, *Water Resour. Res.*, *25*(10), 2109–2118.

Schroth, M. H., J. D. Istok, and J. S. Selker (1998), Three-phase immiscible fluid movement in the vicinity of textural interfaces, *J. Contam. Hydrol.*, *32*, 1–23.

Stauffer, F., and T. Dracos (1986), Experimental and numerical study of water and solute infiltration in layered porous media, *J. Hydrol.*, *84*, 9–34.

Ursino, N., and T. Gimmi (2004), Combined effect of heterogeneity, anisotropy and saturation on steady state flow and transport: Structure recognition and numerical simulation, *Water Resour. Res.*, *40*, W01514, doi:10.1029/2003WR002180.

Ursino, N., T. Gimmi, and H. Flühler (2001a), Combined effects of heterogeneity, anisotropy, and saturation on steady flow and transport: A laboratory sand tank experiment, *Water Resour. Res.*, *37*, 201–208.

Ursino, N., T. Gimmi, and H. Flühler (2001b), Dilution of non reactive tracers in variably saturated sandy structures, *Adv. Water Resour.*, *24*, 877–885.

Vanderborght, J., P. Gähwiller, H. Wydler, U. Schultze, and H. Flühler (2002), Imaging fluorescent dye concentrations on soil surfaces: Uncertainty of concentration estimates, *Soil Sci. Soc. Am. J.*, *66*, 760–773.

van Genuchten, M. T. (1980), A closed-form equation for predicting the hydraulic conductivity of unsaturated soils, *Soil Sci. Soc. Am. J.*, *44*, 892–898.

Walter, M. T., J.-S. Kim, T. S. Steenhuis, J.-Y. Parlange, A. Heilig, R. D. Braddock, J. S. Selker, and J. Boll (2000), Funneled flow mechanisms in a sloping layered soil: Laboratory investigation, *Water Resour. Res.*, *36*, 841–850.

Wildenschild, D., and K. H. Jensen (1999), Laboratory investigations of effective flow behavior in unsaturated heterogeneous sands, *Water Resour. Res.*, *35*(1), 17–28.

H. Flühler, P. Lehmann, and M. Rossi, Institute of Terrestrial Ecosystems, ETH Zurich, Universitätstrasse 16, CH-8092 Zurich, Switzerland. (michela.rossi@env.ethz.ch)

O. Ippisch, Interdisciplinary Center for Scientific Computing, Ruprecht-Karls-University of Heidelberg, D-69117 Heidelberg, Germany.

N. Ursino, Dipartimento IMAGE, Università di Padova, via Loredan 20, I-35131 Padova, Italy.